THE JOURNAL OF BIOLOGICAL CHEMISTRY VOL. 290, NO. 32, pp. 19433–19444, August 7, 2015

Leucine-rich Repeat Kinase 2 (LRRK2) Pharmacological Inhibition Abates α-Synuclein Gene-induced Neurodegeneration*

Received for publication, April 17, 2015, and in revised form, June 5, 2015 Published, JBC Papers in Press, June 15, 2015, DOI 10.1074/jbc.M115.660001

João P. L. Daher[‡], Hisham A. Abdelmotilib[‡], Xianzhen Hu[‡], Laura A. Volpicelli-Daley[‡], Mark S. Moehle[‡], Kyle B. Fraser[‡], Elie Needle[§], Yi Chen[§], Stefanus J. Steyn[¶], Paul Galatsis[‖], Warren D. Hirst[§], and Andrew B. West[‡1]

From the [‡]Center for Neurodegeneration and Experimental Therapeutics, Department of Neurology, The University of Alabama at Birmingham, Birmingham, Alabama 35294, the [§]Pfizer Neuroscience Research Unit, Cambridge, Massachusetts, [¶]Pfizer Pharmacokinetics, Dynamics, and Metabolism Cambridge, Cambridge, Massachusetts 02139, and [‖]Pfizer Worldwide Medicinal Chemistry, Cambridge, Massachusetts 02139

Background: LRRK2 kinase activity has been implicated in Parkinson disease (PD).
Results: LRRK2 kinase inhibition attenuated neurodegeneration in LRRK2 transgenic and wild-type rats.
Conclusion: Chronic inhibition of LRRK2 kinase activity is well tolerated in rats and provides neuroprotection from α-synuclein overexpression.
Significance: These results warrant further studies that test the therapeutic potential of LRRK2 kinase inhibitors in additional PD models.

Therapeutic approaches to slow or block the progression of Parkinson disease (PD) do not exist. Genetic and biochemical studies implicate *α-synuclein* and *leucine-rich repeat kinase 2* (*LRRK2*) in late-onset PD. LRRK2 kinase activity has been linked to neurodegenerative pathways. However, the therapeutic potential of LRRK2 kinase inhibitors is not clear because significant toxicities have been associated with one class of LRRK2 kinase inhibitors. Furthermore, LRRK2 kinase inhibitors have not been tested previously for efficacy in models of *α-synuclein*-induced neurodegeneration. To better understand the therapeutic potential of LRRK2 kinase inhibition in PD, we evaluated the tolerability and efficacy of a LRRK2 kinase inhibitor, PF-06447475, in preventing α-synuclein-induced neurodegeneration in rats. Both wild-type rats as well as transgenic G2019S-LRRK2 rats were injected intracranially with adeno-associated viral vectors expressing human α-synuclein in the substantia nigra. Rats were treated with PF-06447475 or a control compound for 4 weeks post-viral transduction. We found that rats expressing G2019S-LRRK2 have exacerbated dopaminergic neurodegeneration and inflammation in response to the overexpression of α-synuclein. Both neurodegeneration and neuroinflammation associated with G2019S-LRRK2 expression were mitigated by LRRK2 kinase inhibition. Furthermore, PF-06447475 provided neuroprotection in wild-type rats. We could not detect adverse pathological indications in the lung, kidney, or liver of rats treated with PF-06447475. These results demonstrate that pharmacological inhibition of LRRK2 is well tolerated for a 4-week period of time in rats and can counteract dopaminergic neurodegeneration caused by acute α-synuclein overexpression.

Parkinson disease (PD)[2] is a common neurodegenerative disorder affecting 7 to 10 million individuals worldwide (1). Significant degeneration of dopaminergic neurons in the substantia nigra pars compacta (SNpc) typically occurs in mid-stages of disease, accompanied by abnormal accumulations of *α-synuclein* in many surviving neurons (2). Although reasonable symptomatic treatments exist for the early stages of disease, there are no therapeutics available that slow or halt disease progression.

Genetic and pathological studies have identified several proteins linked to PD. Extremely rare missense mutations and gene multiplications in *α-synuclein* result in familial PD, and genome-wide association studies show that *α-synuclein* is the most important genetic susceptibility factor (3, 4). Genetic studies also implicate *leucine-rich repeat kinase 2* (*LRRK2*). The most prevalent *LRRK2* mutation, G2019S, may upregulate LRRK2 kinase activity and is the most common known genetic cause of PD (5, 6).

Further elucidation of the pathobiological mechanisms that link *LRRK2* and *α-synuclein* in PD may be required for the development of targeted therapeutic approaches. LRRK2 kinase activity is thought to regulate the toxic effects of overexpressed G2019S-LRRK2 protein (7). Several strains of mice that express G2019S-LRRK2 protein have been developed, but there are conflicting results with respect to (A53T)α-synuclein neurotoxicity (8–10). Although dopaminergic neurodegeneration

* This work was supported, in whole or in part, by NINDS/National Institutes of Health Grants F31 NS081963 (to M. S. M.), T32 GM00811127 (to K. B. F.), and R01 NS064934 (to A. B. W.). This work was also supported by the Michael J. Fox Foundation for Parkinson's Disease Research (to A. B. W. and W. D. H.) and the American Parkinson's Disease Association (to J. P. L. D. and L. A. V.). E. N., Y. C., S. J. S., P. G., and W. D. H. are employees of Pfizer Inc., which holds patent rights to PF-06447475.
[1] To whom correspondence should be addressed: 1719 6th Ave. S., Birmingham, AL 35294. Tel.: 205-996-7697; Fax: 205-996-6580; E-mail: abwest@uab.edu.

[2] The abbreviations used are: PD, Parkinson disease; SNpc, substantia nigra pars compacta; BAC, bacterial artificial chromosome; rAAV, recombinant adeno-associated virus; TH, tyrosine hydroxylase; iNOS, inducible nitric oxide synthase.

is a key phenotype associated with PD, the α-synuclein transgenic mice utilized so far in LRRK2 studies do not show loss of these cells. The effects of G2019S-LRRK2 and LRRK2 kinase activity on α-synuclein-induced dopaminergic neurodegeneration have not been reported previously but could yield important insights into LRRK2 function in disease.

Transgenic rats expressing G2019S-LRRK2 from a human-derived bacterial artificial chromosome (BAC) have recently been developed and described. Although endogenous LRRK2 localization in rat brains appears to have little overlap with human brains, these transgenic rats display LRRK2 expression in a manner consistent with the human brain (11). The G2019S-LRRK2 rats show very mild motor impairments, potentially because of altered striatal dopamine signaling, but have normal numbers of dopamine neurons in the SNpc and do not show evidence of progressive neurodegenerative phenotypes (12, 13).

The recombinant adeno-associated viral (rAAV) α-synuclein overexpression model of PD faithfully induces dopaminergic neurodegeneration in mice, rats, and non-human primates (14, 15). We found previously that LRRK2 knockout rats are protected from neurodegeneration (16). In that study, we hypothesized that LRRK2 kinase inhibition might phenocopy neuroprotection associated with LRRK2 deficiency. However, a recent study in mice, rats, and non-human primates using one series of LRRK2 kinase inhibitors shows serious adverse effects associated with long-term (*e.g.* 4-week) LRRK2 kinase inhibition (17). Additionally, LRRK2 knockout rats and mice show pathologies in the lung and kidney that include LAMP2-postive organelle accumulation in type II pneumocytes in lung and renal tubule cells in the kidney (18, 19). For these reasons, the therapeutic potential of LRRK2 kinase inhibitors needs additional clarification in animal models.

To determine the effect of G2019S-LRRK2 expression in α-synuclein induced dopaminergic neurodegeneration, we transduced G2019S-LRRK2 expressing rats and wild-type rats with α-synuclein virus and treated these animals with a newly described brain-penetrant LRRK2 kinase inhibitor. Unlike previous LRRK2 inhibitor series that show limited brain permeability, selectivity, and tolerability in rats (17), PF-06447475 shows excellent selectivity and brain penetrance and allows for continuous oral dosing. Overall, we see potent neuroprotection that may reflect a delay or a block in neurodegenerative phenotypes associated with α-synuclein overexpression. Importantly, no adverse effects associated with PF-06447475 administration could be detected in lungs and kidneys.

Experimental Procedures

Statement on Ethics—All experiments involving animals were performed at sites accredited by the Association for Assessment and Accreditation of Laboratory Animal Care International, and all procedures were approved by the local Institutional Animal Care and Use Committees. Experimental compounds were provided by Pfizer Inc. to the University of Alabama at Birmingham under a research agreement approved by Pfizer Inc. and the University of Alabama Research Foundation and The Board of Trustees of the University of Alabama.

Animals—The G2019S-LRRK2 rat (NTac:S.D.-Tg(LRRK2*G2019S)571Cjli, Taconic Farms) was developed at Cornell University by C. J. Li and supported for distribution and licensing by the Michael J. Fox Foundation for Parkinson's Disease Research, who sponsored the work. Transgene-negative littermate controls and hemizygous-positive rats were used for parts of this study. We previously evaluated G2019S-LRRK2 protein expression and localization in these strains of rats (11). Comparable WT-LRRK2 human BAC rats have not been created. Therefore, we utilized an outbred wild-type Sprague-Dawley rat cohort obtained from Charles River Laboratories to study the effects of LRRK2 kinase inhibition in wild-type rats, distinct from the G2019S-LRRK2 strain.

All surgeries were performed on 10- to 12-week-old animals. All rats were maintained on an *ad libitum* diet during the experiments, and cage densities were followed according to the Guide for the Care and Use of Laboratory Animals. Genotyping of NTac:S.D.-Tg(LRRK2*G2019S)571Cjli was accomplished with the forward primer GAT AGG CGG CTT TCA TTT TTC C and the reverse primer ACT CAG GCC CCA AAA ACG AG using Phusion TaqDNA polymerase (New England Biolabs).

Virus Production and Surgeries—Recombinant adeno-associated virus 2/1 (rAAV2/1)-α-synuclein was obtained from the Virus Core of the University of North Carolina and has been described previously (16). Intracranial viral or vehicle control injections were conducted under isoflurane anesthesia using a digital stereotaxic frame (David Kopf) with a thermal adjustable height stage (Physiotemp). Viral stocks were diluted into PBS (pH 7.4) at the specified titer before injection. All rats received a single unilateral 4-μl injection over the course of 20 min using a 32-gauge custom needle (Hamilton) with a 110° bevel fitted to a gas-tight syringe and controlled by a digital pump (Harvard Apparatus). Solutions were injected into the right SNpc at the following empirically derived coordinates: 4.65 mm posterior and 2.25 mm lateral to the bregma and 7.45 mm ventral relative to the skull, with the needle bevel facing laterally. Scalp incisions were closed by suture, and animals were monitored for successful recovery, with food and water consumption expected in the first few hours post-surgery.

Drug Treatments—Drugs coded as compound 1 and 2 were produced by Pfizer Inc. and supplied to investigators at the University of Alabama at Birmingham for this study. Drugs were administered to the desired amount in a suspension solution consisting of 10% propylene glycol (Sigma), 20% PEG-400 (Sigma), and 70% 0.5% methylcellulose (Sigma) using stainless feeding needles 16-gauge curved 3.00 mm ball points (Braintree Scientific, Inc). After study completion and final data analysis, compound 1 was revealed to be calcium carbonate and function as the control compound, and compound 2 was revealed to be PF-06447475. Both compounds have an identical appearance, bright white, loosely packed powder, and have identical profiles in the vehicle.

LC/MS/MS—Liquid chromatography and tandem mass spectrometry analyses were used to calculate all drug concentrations in biofluids and tissues. Quantization was performed for PF-06447475 using transitions of m/z 304.2 → 258 normalized to the internal standard indomethacin (m/z 356.1 → 312.1).

Pharmacodynamic Assays—Rat tissues or cell line pellets were homogenized in lysis buffer consisting of 50 mM Tris (pH

7.4), 150 mM NaCl, 1.5 mM $MgCl_2$, 5% glycerol, 1 mM Na_3VO_4, 25 mM NaF, 1 mM DTT, 0.8% Nonidet P-40, and 0.5 mM PMSF, with one Complete protease tablet and one PhosStop tablet per 10 ml of lysis buffer (Roche). After homogenization, lysates were centrifuged at ~20,000 × *g* for 15 min at 4 °C. Proteins were electrophoresed on 3–8% Tris acetate midi gels and then transferred onto Immobilon-FL membranes (Millipore) and blocked with near infrared buffer (Rockland). Membranes were probed with two LRRK2 antibodies, 100–500 (1:2000, Abcam) and MJFF3 (1:1000, Abcam), in addition to Ser(P)-935 (1:2000, Abcam). Membranes were scanned, and band intensities were quantified using the LI-COR Odyssey system. Calculation of LRRK2 kinase inhibition was made by determining the ratio of Ser(P)-935 to total LRRK2 by applying both antibodies to membranes at the same time and simultaneous scanning with 685-nm and 785-nm lasers, respectively (IRDye 650 goat anti-rabbit and IRDye 800 goat anti-mouse).

Immunohistochemistry—Brain sections were prepared for immunochemistry and analyzed as described previously (11). The following primary antibodies were used on tissue sections: anti-nitrosylated/oxidized α-synuclein syn514 (courtesy of Virginia Lee), anti-tyrosine hydroxylase (TH, Sigma, and Santa Cruz Biotechnology), anti-rat CD68 (AdSerotec), anti-Iba1 (rabbit polyclonal, 1:500, Wako), anti-MHC-II (clone Ox6, mouse monoclonal, AbSerotec), anti-iNOS (BD Biosciences), and LRRK2 (clone N241, Antibodies Inc.). Brain sections were prepared from paraformaldehyde-fixed, sucrose-embedded brains. Confocal images were captured by a single observer blinded to the experimental conditions (drug treatment group and genotype status) using a Leica TCS-SP5 laser-scanning confocal microscope. The Leica LASAF software, Adobe Photoshop (contrast, brightness, and color adjustments), and Adobe Illustrator were used to create figures and process images. Iba1 immunoreactivity (*i.e.* microgliosis) was calculated from confocal images captured from sections spaced 120 μm apart across the entire SNpc using a ×20 objective, and occupancy of Iba1 reactivity was calculated with ImageJ software. Immunofluorescence of TH in the dorsal striatum was quantified using a LI-COR Odyssey scanner with images processed and quantified by Image Studio 4 software. For 3,3′-diaminobenzidine-stained sections, the avidin-biotin complex reagent kit, together with ImmPACT substrate (Vector Labs), was used. Sections were counterstained with Nissl using a standard protocol, and images were captured with an Olympus BX61 BF microscope.

Histological and Pathological Stains—Sucrose-embedded organs (lung, kidney, spleen, and liver) were paraffinized and sectioned on a microtome to 10-μm thickness (Leica). Sections were deparaffinized, rehydrated, and processed into hematoxylin stain (no. 7211, Richard-Allen Scientific) and eosin stain (Vector Labs). Oil Red O stain (Sigma) was applied to frozen sections cut at 10-μm thickness and counterstained with Gill's hematoxylin (Richard-Allen Scientific). Masson's trichome stain (Sigma) was used with paraffin sections at 5-μm thickness and post-fixed in Bouin's fixative (Sigma). Slides were stained with Weigert's hematoxylin (Sigma), followed by staining in Biebrich scarlet-acid fuchsin solution (Sigma) for differentiation. Some sections were stained with aniline blue.

Sections from rat spleen, liver, lung, and kidney were deparaffinized, hydrated, and subjected to antigen retrieval using preheated 10 mM sodium citrate buffer (pH 6) with a pressure cooker for 5 min for CD68 staining and in 10 mM Tris-1 mM EDTA buffer (pH 9) for LAMP2. Sections were incubated with 3% hydrogen peroxide for 10 min, blocked in normal serum, and incubated with antibodies to LAMP2 (Santa Cruz Biotechnology) and CD68 (clone ED1, AbD Serotec). DAB chromagen (Scy Tek Laboratories) and hematoxylin (no. 7211, Richard-Allen Scientific) were used to stain the sections.

Stereology—Unbiased stereological estimation of the total number of TH+, Nissl+, or CD68+ cells in the SNpc was performed using an optical fractionator probe (MicroBrightField) by an investigator blinded to the identity of the experiment. A low-power objective was used to delineate the borders of the SNpc, identified through Nissl contrast stain, at all midbrain levels. Sections used for counting covered the entire SNpc and were spaced equally, 120 μm apart, with the counting frame placed randomly on the first counting area and moved systematically through all counting areas until the entire delineated region was sampled. The density of counting frames was adjusted so that at least 100 objects were counted for each observation, with most estimations made on the basis of >200 objects counted per estimation.

Statistics—Statistical analysis and graphs were performed and created with GraphPad Prism 6.0 software. Experimental groups were confirmed for normality using the Kolmogorov-Smirnov test and homogeneity of variances using Levene's test. Two-tailed unpaired Student's *t* tests and one-way analysis of variance were used to calculate *p* values, where less than 0.05 was considered significant.

Results

G2019S-LRRK2 Expression Exacerbates α-Synuclein-induced Dopaminergic Neurodegeneration—To determine the effects of G2019S-LRRK2 expression on α-synuclein-induced dopaminergic neurodegeneration, G2019S-LRRK2 rats (G2019S+) or littermate non-transgenic controls (G2019S-) were unilaterally injected with rAAV2/1-α-synuclein virus. The timeline for dopaminergic neurodegeneration in this model system has been established previously (15, 16, 20). We first evaluated rats 2 weeks post-viral transduction for human α-synuclein expression, before the onset of neurodegeneration. Confocal imaging revealed comparable transduction efficiencies and expression of human α-synuclein across the injected SNpc in both G2019S+ and G2019S− rats (Fig. 1*A*), with TH staining and distribution indistinguishable from the uninjected SNpc.

α-Synuclein protein normally localizes to presynaptic termini (21, 22). Acute overexpression of α-synuclein in SNpc neurons results in the accumulation of nitrosylated/oxidized α-synuclein in the soma of surviving dopaminergic neurons 4 weeks post-viral transduction (15, 16, 23). Analysis of serial brain sections for nitrosylated/oxidized α-synuclein demonstrated abundant abnormal α-synuclein in the soma of surviving TH+ neurons in both G2019S+ and G2019S− rats (Fig. 1, *B* and *C*). Stereological counts of TH cells in the injected side (ipsilateral) and uninjected side (contralateral) revealed an ~20% loss of TH positive neurons in G2019S− rats (Fig. 1*E*).

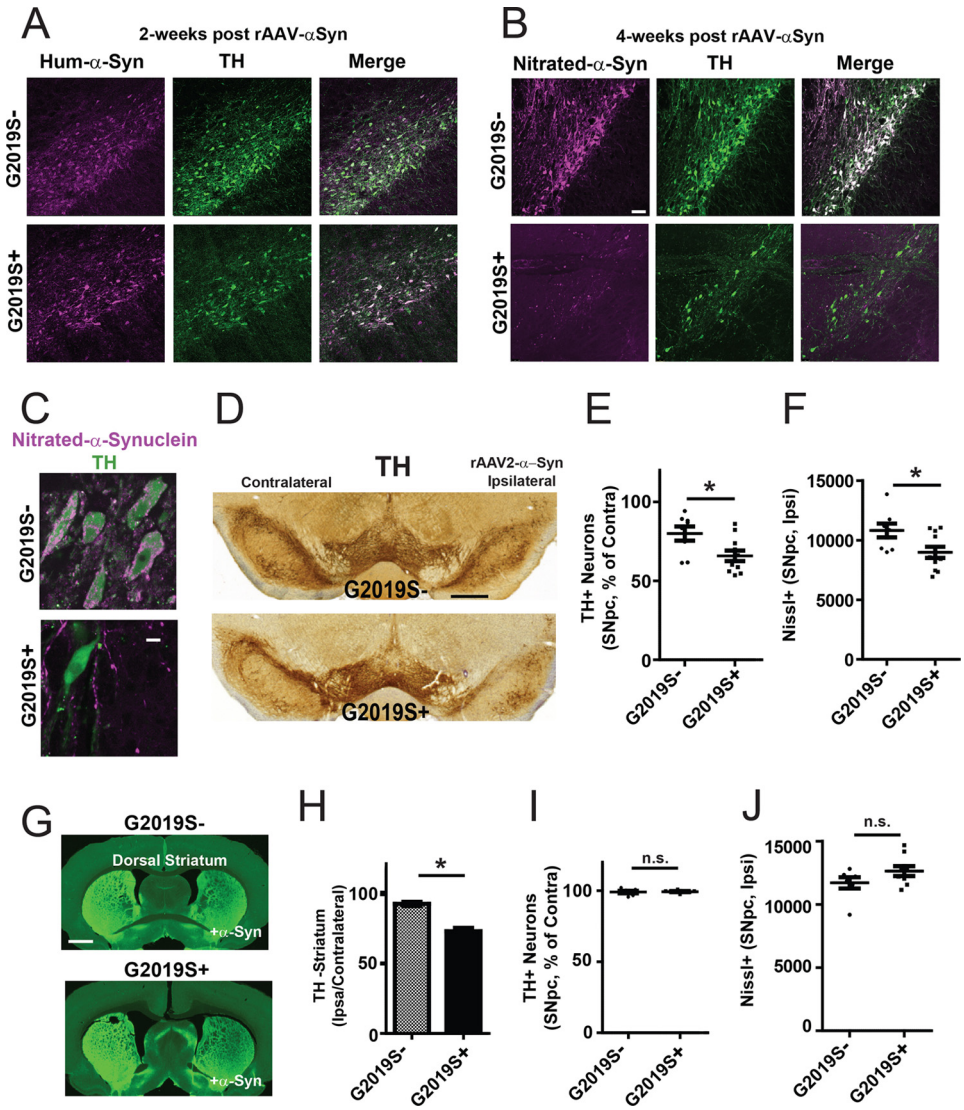

FIGURE 1. **G2019S-LRRK2 expression enhances α-synuclein-induced dopaminergic neurodegeneration.** Analysis of a rat cohort derived from hemizygous hBAC G2019S-LRRK2 transgenics mated with Sprague-Dawley Taconic Farms outbred animals. 10- to 12-week-old rats were unilaterally injected with 6×10^9 rAAV2 α-synuclein viral particles. *A*, three G2019S+ and G2019S− (littermate transgene-negative controls) rats were sacrificed 2 weeks post-injection and analyzed for human α-synuclein and TH expression. >90% viral transduction of TH-positive cells was observed across the SNpc in all animals. Representative confocal sections are shown for α-synuclein (human isoform-specific, Syn211 monoclonal, *magenta*) and TH (*green*) expression in the SNpc. No differences could be observed between the two groups. *B*, a cohort of 19 rats ($n = 8$, G2019S−; $n = 11$, G2019S+) were sacrificed 4 weeks post-injection and analyzed for abnormal nitrated/oxidized α-synuclein (Syn514 monoclonal) and TH expression in surviving SNpc cells using confocal analysis. Representative images are shown. *C*, a representative high-magnification image of nitrated/oxidized α-synuclein in TH-positive neurons in the SNpc. *D*, representative coronal DAB-stained sections showing TH immunoreactivity in the SNpc with Nissl counterstain with respect to ipsilateral injection of rAAV2 α-synuclein viral particles as indicated. *E*, unbiased stereology counts of TH-positive neurons in the SNpc normalized to TH-positive neuron counts on the contralateral side. *F*, raw counts of Nissl-positive cells in the ipsilateral (injected) side of G2019S− and G2019S+ rats. *G*, representative images showing TH fiber density in the striatum. *H*, quantification of dorsal striatum TH fiber density calculated from 27 sections using LI-COR analysis (derived from the animals analyzed in *E*). *I*, stereological counts of TH-positive cells in the SNpc in an equivalently aged and separate cohort of rats consisting of nine G2019S+ rats and seven G2019S− littermate controls, analyzed after sham surgery control (vehicle injection, ipsilateral). *J*, raw counts of Nissl-positive cells on the ipsilateral (injected) side of G2019S− and G2019S+ rats. All stereological counts were performed by investigators blinded to the genetic identity of the rats. *Scale bars* = 100 μm (*A* and *B*), 5 μm (*C*), and 0.5 mm (*D* and *F*). *, $p < 0.02$ as calculated with a two-tailed unpaired Student's *t* test; *n.s.*, not significant. Data are means ± S.E.

This lesion size is consistent with observations made previously in the Long-Evans outbred background injected with the same concentration and pseudotype of virus expressing human wild-type α-synuclein (16). In contrast, an ~40% loss of TH-positive neurons in the SNpc could be observed in G2019S+ rats. Direct comparison of Nissl+ cell counts through the SNpc confirmed the loss of neurons in G2019S+ and G2019S− rats, as opposed to a loss of TH expression (Fig. 1*F*). TH fiber density in the ipsilateral dorsal striatum was also reduced significantly in G2019S+ compared with G2019S− rats (Fig. 1, *G* and *H*).

To ensure that the surgical procedure and injection of the viral suspension vehicle did not produce the exacerbated neurodegeneration we find in G2019S+ rats, we analyzed a separate cohort of rats unilaterally injected with vehicle solution (Fig. 1, *I* and *J*). Stereological estimations of TH- and Nissl-positive cells revealed that the surgical procedure itself did not result in a loss of TH cells in either G2019S+ or G2019S− rats,

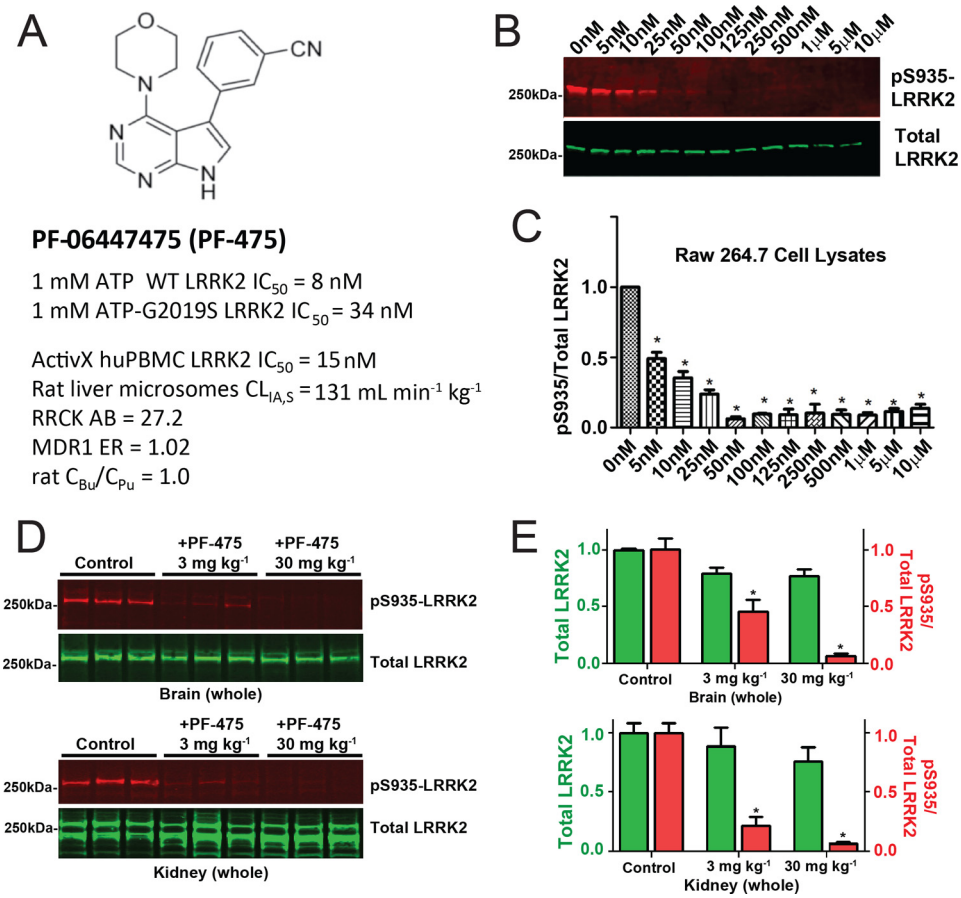

FIGURE 2. **Efficacy and pharmacodynamic properties of the LRRK2 kinase inhibitor PF-06447475.** *A*, the structure of PF-06447475. LRRK2 kinase inhibitory activity was measured using recombinant full-length, GST-tagged LRRK2 protein and LRRKtide as a surrogate kinase substrate in a FRET assay in the presence of 1 mM ATP. The inhibitory potential was also calculated with a commercial ActivX assay in human peripheral blood monocytic cells (*PBMCs*). Rat liver microsome stability, passive permeability (*RRCK cells*), and P-gp efflux ratios (*MDR1 cells*) are shown. Brain availability is indicated by equivalency in rat unbound brain concentrations (C_{Bu}) to unbound plasma concentrations (C_{Pu}). *B*, cells from the mouse macrophage cell line raw 264.7 were treated with the indicated concentration of PF-06447475 for a period of 24 h before protein lysate generation and analysis for Ser(P)-935 and total LRRK2 expression by Western blot. *C*, a half-maximal inhibitor concentration was observed at ~5 nM with respect to the ratio of Ser(P)-935 to total LRRK2 levels. *D*, groups of six (three male and three female) Sprague-Dawley rats were treated with PF-06447475 or vehicle control (p.o. b.i.d.) for 14 days and sacrificed 90 min after the last dose. Whole brains and kidneys were removed rapidly and processed to protein lysates to quantify Ser(P)-935-LRRK2 and total LRRK2. Signals from 50 μg of total protein, as determined by BCA assay, were analyzed per lane. *E*, quantification of the LRRK2 signal and the ratio of Ser(P)-935 to total LRRK2 in both brain and kidney. *, $p < 0.01$, calculated by one-way analysis of variance with Tukey's post-hoc test (*C* and *E*). All other group comparisons were not significant ($p > 0.05$) compared with control groups (Tukey's post hoc test). Data are means ± S.E.

and, as expected, the SNpc Nissl cell counts were not different between G2019S+ and G2019S− rats. This is consistent with previous studies reporting that G2019S-LRRK2 rats have normal numbers of SNpc cells (12, 13).

The Novel LRRK2 Inhibitor PF-06447475 Is Well Tolerated in Rats—Through drug screening and chemistry efforts, a novel small molecule LRRK2 inhibitor, PF-06447475, was discovered (Fig. 2*A*). This inhibitor shows low nanomolar affinity for LRRK2 in cells and tissues (Fig. 2, *B–E*) and shows minimal inhibition of other kinases (24). Analysis of plasma and brain lysates after oral administration of PF-06447475 shows similar concentrations of unbound compound, demonstrating exceptional brain permeability of the drug (24). Cellular IC_{50} values for endogenous LRRK2 kinase activity in the macrophage cell line Raw264.7 are less than 10 nM (Fig. 2*B*), demonstrating the potency of the compound.

To determine the potency of PF-06447475 in blocking brain LRRK2 kinase activity, wild-type Sprague-Dawley rats were treated at 3 and 30 mg·kg^{-1} PF-06447475 (p.o. b.i.d.) for 14 days, and total and phospho-LRRK2 were subsequently measured from brain tissue lysates (Fig. 2*D*). In brain and kidney tissue homogenates obtained 90 min from the last drug administration, both 3 and 30 mg·kg^{-1} PF-06447475 significantly reduced the ratio of Ser(P)-935 LRRK2 to total LRRK2 protein, whereas total LRRK2 protein was not reduced significantly in either tissue compared with vehicle control tissue (Fig. 2*E*). Pharmacokinetic profiles of PF-06447475 administered at 30 mg·kg^{-1} p.o. b.i.d. resulted in unbound drug concentrations in the brain above the C_{eff} level (15 nM, Ref. 24) at all times. With 30 mg·kg^{-1} p.o. b.i.d., plasma $C_{max,u}$ was 380 nM (25-fold above C_{eff}) and plasma-unbound concentration time curve was 4140 nM hour^{-1} (11-fold above C_{eff}). Therefore, a 30 mg·kg^{-1} p.o. b.i.d. was selected as an appropriate dosage regimen to determine the effects of LRRK2 kinase inhibition in rats because this concentration maintains an IC_{50} level of drug continuously. Notably, these dosages and concentrations of LRRK2 inhibitor are much lower than those described previously to achieve the same level of LRRK2 brain inhibition (17).

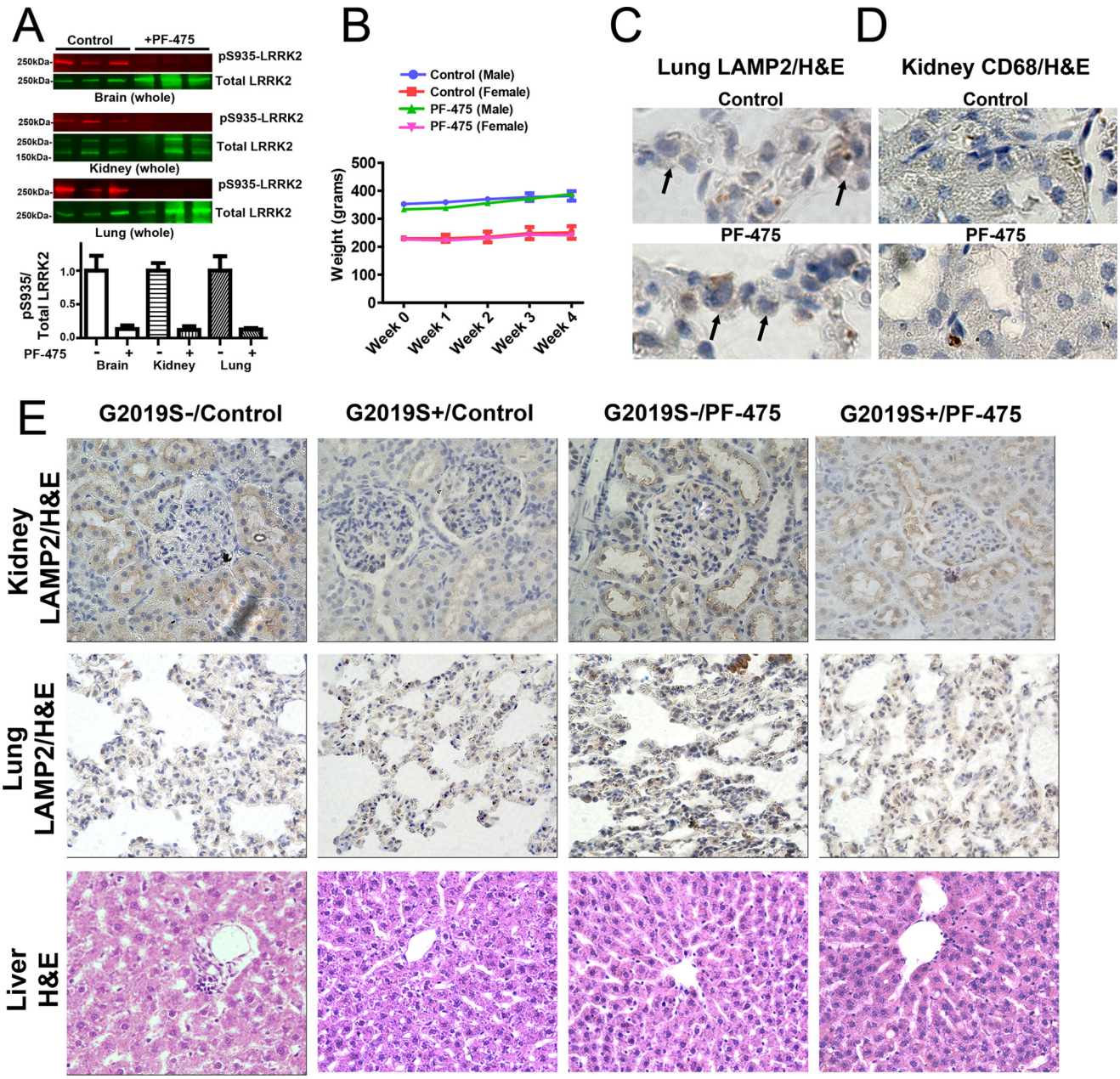

FIGURE 3. **LRRK2 kinase inhibition is well tolerated in rats.** 10- to 12-week-old male Sprague-Dawley G2019S-LRRK2 BAC transgenic G2019S+ rats and non-transgenic G2019S− controls were treated at 30 mg·kg^{-1} b.i.d. by oral gavage with either PF-06447475 (PF-475) or control compound. *A*, tissues, including whole brain, kidney, and lung, were harvested from G2019S− rats treated with PF-06447475 or control 2 h post-oral gavage. Tissues were immediately processed into lysates for calculation of LRRK2 kinase inhibition (*i.e.* pS935/LRRK2 ratio) as determined by LI-COR analysis. $n = 3$ rats/group. *B*, weights from G2019S− rats were recorded at baseline and weekly, as indicated, with mean values shown calculated from at least 3 rats/group (*error bars* are mean ± S.E.). Weights from G2019S+ rat groups were not significantly different from G2019S− groups and, likewise, did not vary with treatment. *C*—*E*, after 4 weeks of drug treatment, at least three perfused rats from each of the four groups (G2019S− and G2019S+, as indicated) were processed into paraffin blocks, and sections from the liver, kidney, lung, and spleen were stained with H&E, Masson's trichrome, LAMP2-DAB, CD68-DAB, and Oil Red O (for lipids, lipofuscin, and lipoproteins). Sections were evaluated by a pathologist blinded to group identity, and all images are representative of sections derived from the 3 rats/group. *C*, representative high-magnification (×63) images of lung tissue highlighting type II pneumocytes (*arrows*) stained with an antibody for LAMP2 (*brown coloration*, DAB stain) with H&E as a contrast stain. *D*, representative high-magnification (×40) images of kidney renal tubules stained for CD68 to highlight myeloid cells (*brown coloration*, DAB-stain) with H&E as a contrast stain. *E*, representative low-magnification (×20) images of the indicated organ with the indicated stain. In all animals and stains, no differences could be detected between the groups.

To determine the effects of PF-06447475 on adverse pathologies previously associated with LRRK2 KO or LRRK2 kinase inhibition, we generated a cohort of G2019S-LRRK2 and wild-type rats treated with PF-06447475 for 4 weeks at 30 mg·kg^{-1} b.i.d. The effects of PF-06447475 on weight changes and abnormalities in the kidney, liver, and lung in both G2019S+ and G2019S− rats were examined. Near complete ablation of Ser(P)-935 LRRK2 levels were observed in the brain, lung, and kidney, as anticipated (Fig. 3*A*). PF-06447475 treatment did not affect the weight of the rats (Fig. 3*B*). We did not observe any differences between control-treated groups and PF-06447475-treated groups using a variety of stains and immunohistochemical assays, as assessed by pathologists blinded to group identity (Fig. 3, *C*–*E*). Specifically, there was normal LAMP2 distribu-

tion in type II pneumocytes in lung and in renal tubule cells in the kidney, and we did not observe abnormal accumulations of CD68 myeloid cells in the kidney, liver, or lung (Fig. 3, *C–E*). Evaluation of liver tissue using Masson's trichrome stain and H&E did not show any evidence of hepatotoxicity caused by PF-06447475 treatment, demonstrating that rats tolerate PF-06447475 well.

PF-06447475 Abates α-Synuclein-induced Dopaminergic Neurodegeneration—To determine whether G2019S-LRRK2 kinase activity is responsible for the exacerbated neurodegeneration associated with viral overexpression of α-synuclein, the 30 mg·kg^{-1} p.o. b.i.d. regimen was applied to G2019S+ rats for the entire 4-week duration of the experiment. A control compound was also administered at equivalent doses by investigators blinded to compound identities. Confocal analysis for nitrosylated/oxidized α-synuclein showed the relative preservation of TH-positive cells with abnormal α-synuclein expression in rats treated with PF-06447475 (Fig. 4, *A* and *B*). Stereological estimations of the number of SNpc TH neurons showed that an ~40% loss of cells occurred in the group of G2019S+ rats treated with the control compound in contrast to no significant loss of TH cells in the SNpc in G2019S+ rats treated with PF-06447475 (Fig. 4*C*). Stereological counts of Nissl+ cells through the SNpc confirmed the neurodegeneration in G2019S+ rats treated with inert control compound compared with G2019S+ rats treated with PF-06447475 (Fig. 4*D*). Treatment of G2019S+ rats with PF-06447475 also preserved TH expression in the dorsal striatum, consistent with drug attenuating neurodegeneration in the SNpc (Fig. 4, *F* and *G*).

Because the level of neuroprotection observed in the G2019S+ rats exceeded the neurodegenerative effects that we could attribute to G2019S-LRRK2 expression (Fig. 1), PF-06447475 was next tested in a cohort of wild-type Sprague-Dawley outbred rats independent from the G2019S-LRRK2 BAC strain (Fig. 4, *H—N*, *G2019S*−). In G2019S− wild-type rats, an ~20% loss of TH neurons in the SNpc occurred in control compound-treated rats, as expected (Fig. 4*J*, consistent with observations in Ref. 16). However, in rats treated with PF-06447475, we could not detect a significant loss of TH neurons (Fig. 4, *J* and *K*), despite the robust expression of abnormal nitrosylated/oxidized α-synuclein across the SNpc of these animals (Fig. 4*I*). One rat in the PF-06447475-treated group demonstrated extreme neurodegeneration (~60% loss of TH cells) and was identified as a biological outlier (extreme studentized deviate, $p < 0.01$) and was excluded from the analysis. Evaluation of TH fiber density in the striatum also demonstrated preservation of dopaminergic axons in the wild-type rats treated with PF-06447475 (Fig. 4, *M* and *N*).

PF-06447475 Attenuates Neuroinflammation Associated with G2019S-LRRK2 Expression—To determine the effect of PF-06447475 on neuroinflammation in both G2019S-LRRK2 and wild-type rats, we measured Iba1 reactivity, a marker of microgliosis, through serial sections across the SNpc using confocal analysis (Fig. 5, *A* and *B*). This approach has been used previously to measure microglial activation in models of Alzheimer disease (25). G2019S-LRRK2 rats show significantly increased microgliosis compared with wild-type rats (Fig. 5*C*), consistent with previous results that show enhanced microgliosis in G2019S-LRRK2 rats in response to LPS exposure (26). In G2019S+ rats treated with PF-06447475, a significant reduction in microgliosis to levels found in wild-type rats could be observed (Fig. 5*C*). The proinflammatory marker MHC-II expressed on myeloid cells but not neurons also appeared to be less abundant in confocal sections in G2019S+ rats treated with PF-06447475 (Fig. 5*A*). Inducible nitric oxide synthase (iNOS) is also expressed in some proinflammatory myeloid cells, and, in some sections of SNpc from G2019S+ rats treated with control drug, Iba1/MHC-II/iNOS-positive cells could be observed. In contrast, iNOS cells could not be detected in the SNpc from G2019S+ rats treated with PF-06447475.

In G2019S− wild-type rats treated with control compound, microgliosis was markedly less pronounced than in G2019S+ rats treated with control compound (Iba1 immunoreactivity of 36.62% ± 2.583% in G2019S+ rats *versus* 14.37% ± 2.345% in G2019S− rats, $p < 0.0001$, two-tailed unpaired Student's *t* test). However, PF-06447475 administration in wild-type rats did not significantly reduce microgliosis, although there was a trend toward a reduction (Fig. 5*C*). MHC-II expression across the SNpc also appeared comparable between wild-type rats treated with PF-06447475 or control, and iNOS cells were not detected in either group.

As opposed to Iba1, which can be expressed in quiescent myeloid cells (*e.g.* surveying microglia), CD68-positive myeloid cells were extremely rare in the non-injected SNpc but were abundant enough to be counted using standard unbiased stereology on the injected SNpc (Fig. 6). Stereological counts of CD68-positive myeloid cells demonstrated that G2019S+ rats treated with control compound only had consistently elevated numbers of cells compared with wild-type G2019S− rats (257,000 ± 35,000 CD68 cells per ipsilateral SNpc in G2019S+ *versus* 129,000 ± 41,000 CD68 cells in G0219S− rats, $p < 0.01$, two-tailed unpaired Student's *t* test). PF-06447475 treatment in G2019S+ rats significantly lowered the number of CD68 cells recruited to the SNpc (Fig. 6*C*). However, PF-06447475 treatment in non-transgenic rats did not significantly affect CD68-positive cell recruitment to the α-synuclein lesion site. Therefore, using immunohistochemical approaches, PF-06447475 successfully blocked the enhanced neuroinflammation associated with G2019S-LRRK2 expression, but we were unable to find evidence that PF-06447475 could modify α-synuclein-associated neuroinflammation in wild-type rats.

Discussion

This study demonstrates that G2019S-LRRK2 expression exacerbates neuroinflammation and dopaminergic neurodegeneration caused by α-synuclein overexpression and that these effects can be abated by the chronic administration of a potent LRRK2 kinase inhibitor. The LRRK2 kinase inhibitor PF-06447475 was also effective at attenuating α-synuclein-induced dopaminergic neurodegeneration in wild-type rats. Finally, the pathologies reported previously with the chronic administration of one series of LRRK2 kinase inhibitors (17) were not reproduced in the animals in this study. Together, these are important observations for designing additional preclinical studies for LRRK2 kinase inhibitors.

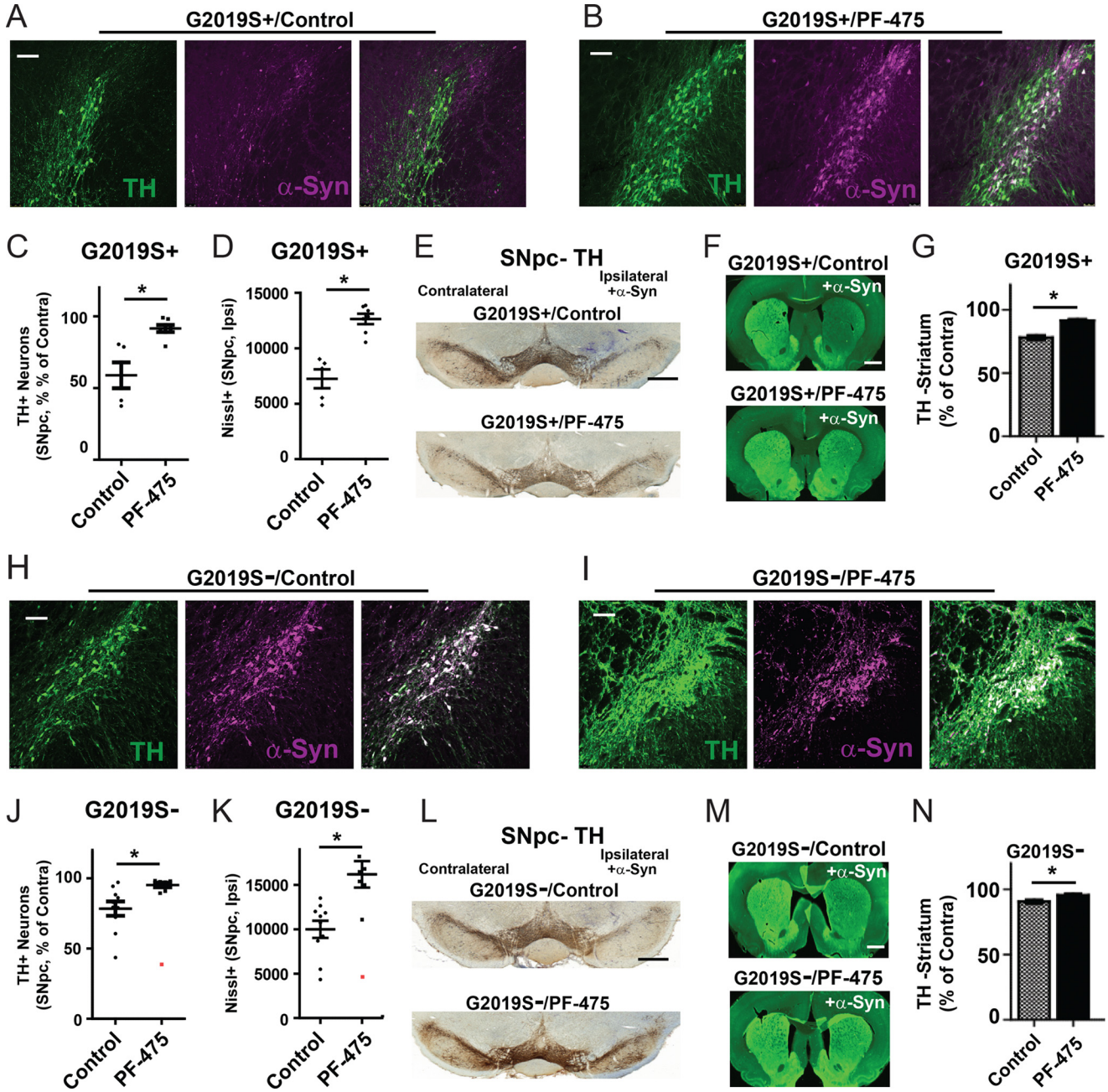

FIGURE 4. **PF-06447475 administration blocks α-synuclein-induced dopaminergic neurodegeneration.** 10- to 12-week-old male G2019S-LRRK2 BAC transgenic rats (G2019S+, $n = 12$) and nontransgenic (WT) rats (G2019S−, $n = 16$) were unilaterally injected with 6×10^9 rAAV2 α-synuclein viral particles. Animals were treated at 30 mg·kg^{-1} b.i.d. by oral gavage with either PF-06447475 (*PF-475*) or a control compound by investigators blinded to compound identity. No animals had adverse events to compound treatments that prevented inclusion in the study. *A* and *B*, representative confocal images of the ipsilateral SNpc with TH stain (*green*) and nitrated/oxidized α-synuclein (*magenta*) given for G2019S+ rats treated with PF-06447475 (*A*) or control compound (*B*). *C*, unbiased stereological analysis of TH-positive neurons in the SNpc with respect to ipsilateral (*ipsi*, injected) and contralateral (*contra*, un-injected) sides. *D*, raw Nissl counts of the ipsilateral (*ipsi*) SNpc as determined by stereology. *E*, representative coronal sections showing TH immunoreactivity in the SNpc with Nissl counterstain. *F*, representative fluorescent images showing TH fiber density in the striatum. *G*, quantification of dorsal striatum TH fiber density, calculated from the evaluation of more than 80 sections from animals in *C*. *H* and *I*, representative confocal images of the ipsilateral SNpc with TH stain and nitrated/oxidized α-synuclein in G2019S- rats treated with control (*H*) or PF-06447475 (*I*). *J*, unbiased stereological counts of TH cells in G2019S− rats with respect to unilateral injection of α-synuclein virus. A biological outlier (extreme studentized deviate test, $p < 0.01$) that demonstrated extreme neurodegeneration and was excluded from the analysis is shown in *red*. *K*, raw Nissl counts for the ipsilateral (injected) side, with the biological outlier identified in *red* and excluded from the statistical analysis as an outlier. *L*, representative coronal sections showing TH immunoreactivity in the SNpc with Nissl counterstain. *M*, representative fluorescent images showing TH fiber density in the striatum. N, quantification of dorsal striatum TH fiber density, calculated from the evaluation of more than 80 sections from animals in *J*. All stereological counts were performed by investigators blinded to the genetic identity and compound treatment groups. *Scale bars* = 0.5 mm (*E* and *L*) and 200 μm (all other panels). *, $p < 0.05$ as calculated with a two-tailed unpaired Student's *t* test. Data are mean ± S.E.

We and others have hypothesized previously that small molecule LRRK2 kinase inhibitors may have therapeutic potential to ameliorate neurodegenerative processes associated with G2019S-LRRK2 (27). The toxic effects of G2019S-LRRK2 in neurons and exacerbating effects on proinflammatory responses are attributed to the enhanced kinase activity associ-

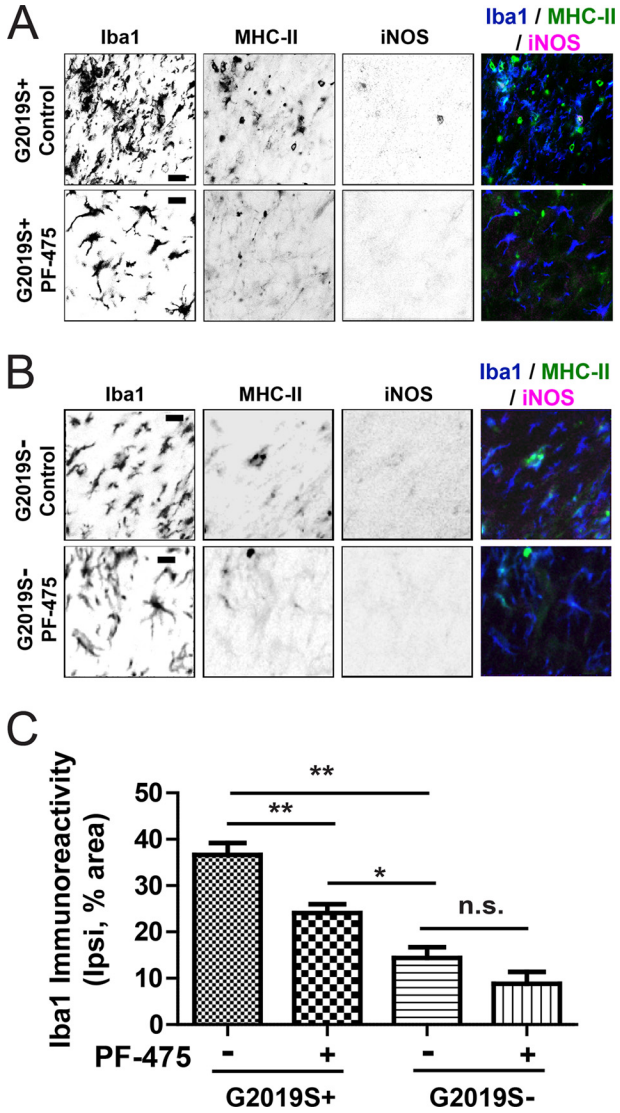

FIGURE 5. **Microgliosis associated with G2019S-LRRK2 expression is attenuated by PF-06447475 in G2019S-LRRK2 rats.** 10- to 12-week-old male G2019S-LRRK2 BAC transgenic rats and G2019S− controls were unilaterally injected with 6×10^9 rAAV2 α-synuclein viral particles and treated with 30 mg·kg^{-1} b.i.d. by oral gavage with either PF-06447475 (*PF-475*) or control compound for 4 weeks. Four rats were analyzed per experimental group by confocal analysis of serial sections across the ipsilateral SNpc for each animal. *A* and *B*, representative confocal sections of the ipsilateral SNpc from G2019S+ rats (*A*) or G2019S− rats triple-stained for Iba1, MHC-II, and iNOS (*B*) in grayscale (to enhance contrast) together with colored merged images (*blue*, Iba1; *green*, MHC-II; *magenta*, iNOS). iNOS-positive cells were not identified in most sections of the SNpc, with the exception of G2019S+ control compound-treated rats. MCH-II- or iNOS-positive cells could not be found in the contralateral side in any group. *C*, fractional area of immunoreactivity for Iba1 calculated from equivalent fields across the SNpc of control or PF-06447475-treated G2019S+ and G2019S− rats. *Scale bars* = 10 μm. *, $p < 0.05$; **, $p < 0.01$; *n.s.*, $p > 0.05$, as calculated with one-way analysis of variance with Tukey's post hoc comparison. Data are mean ± S.E.

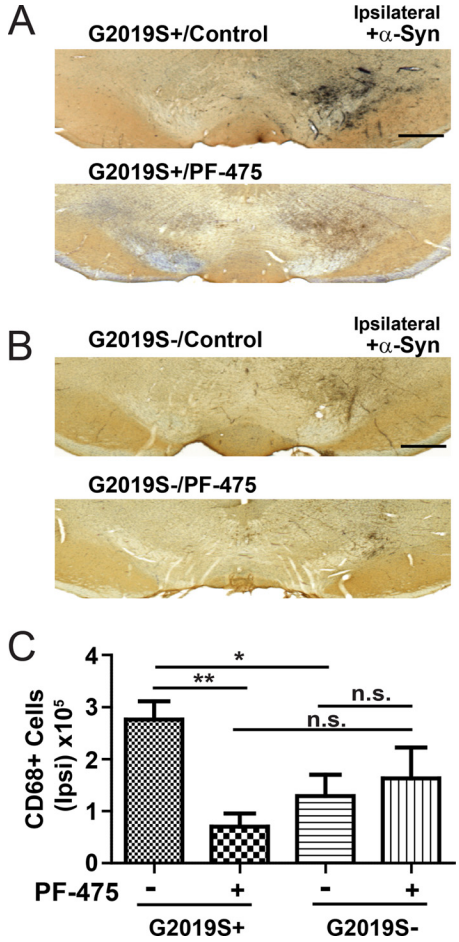

FIGURE 6. **Reduced CD68 cell recruitment in G2019S-LRRK2 rats treated with PF-06447475.** 10- to 12-week-old male G2019S-LRRK2 BAC transgenic rats and G2019S− controls were unilaterally injected with 6×10^9 rAAV2 α-synuclein viral particles and treated with 30 mg·kg^{-1} b.i.d. by oral gavage with either PF-06447475 (*PF-475*) or control compound for 4 weeks. At least four rats were analyzed per experimental group by analysis of serial sections across the ipsilateral SNpc. *A* and B, representative coronal sections DAB-stained for CD68 with Nissl counterstain in G2019S+ (*A*) or G2019S− rats (*B*). *C*, stereological counts of CD68-positive cells across the ipsilateral midbrain in G0219S+ and G2019S− rats treated with control or PF-0644747 compounds. CD68 counts were always below 100 across the contralateral SNpc and did not vary between groups. *Scale bars* = 0.5 mm. *, $p < 0.05$; **, $p < 0.01$; *n.s.*, $p > 0.05$, as calculated with one-way analysis of variance with Tukey's post hoc comparison. Data are mean ± S.E.

ated with the G2019S mutation (26, 28, 29). The efficacy we observed for PF-06447475 in abating α-synuclein neurodegeneration in wild-type rats was surprising to us given the restricted nature of LRRK2 expression in the rat brain (11). The PF-06447475 compound utilized here demonstrates a clear superiority in potency, specificity, and bioavailability compared with other published LRRK2 kinase inhibitors, so an informative cross-comparison with other LRRK2 inhibitors was not possible. PF-06447475 demonstrates some cross-reactivity with the STE20 family of protein kinases (24). One route to establish on-target effects for PF-06447475 neuroprotection would be to utilize the same rAAV2 α-synuclein model in LRRK2 KO rats. However, LRRK2 KO rats appear to be fully protected from rAAV2 α-synuclein-induced neurodegeneration (16). We propose that PF-06447475 serves as a benchmark compound for testing the efficacy of LRRK2 kinase inhibition in neuroprotection, with the caveat that off-target neuroprotective effects could not be fully accounted for in our study.

A recent report, published during the course of our studies, suggested that there might be significant toxicities associated with LRRK2 kinase inhibition, particularly in rats (17). In fact, one of the two related LRRK2 inhibitors that advanced to non-human primates was lethal when administered to rats (17). This series of inhibitor also reduced total LRRK2 protein levels in

multiple tissues. Because of this report, but also data generated from LRRK2 KO rats, we generated a cohort of rats for the purpose of assessment of all pathologies previously attributed to the loss of LRRK2 expression or activity. However, PF-06447475 treatment for a 4-week period of time did not result in any of the expected abnormalities observed in LRRK2 KO rats or non-human primates treated with LRRK2 kinase inhibitors (17, 18). In addition, PF-06447475 had mild or no effects on reducing total LRRK2 protein in brain and kidney homogenates.

Our results cannot be explained by a lack of LRRK2 kinase inhibition because the dosage regimen selected here achieved IC_{90} inhibition for ~18 h per day in the rat brain and levels continuously above IC_{50} for LRRK2 kinase activity. However, this level of inhibition is clearly different from a complete ablation of LRRK2 expression as in the LRRK2 KO. Although we did not observe strong effects of PF-06447475 in reducing LRRK2 expression, it is possible that the treatment reduced G2019S-LRRK2 expression in particular cell subtypes to derive some or all of the observed neuroprotective benefits. However, in whole brain and tissue homogenates, LRRK2 expression was preserved and, therefore, different from LRRK2 KO animals that harbor kidney and lung abnormalities. It also remains possible that rats do not faithfully mimic undesirable pathologies that appear in non-human primates treated with LRRK2 kinase inhibitors or that we did not treat the rats long enough to visualize these undesirable effects. Nevertheless, we are encouraged that all groups of rats we analyzed tolerated PF-06447475 treatment well with no apparent adverse effects.

The viral model of α-synuclein utilized here has provided important clues relevant to α-synuclein neurotoxicity. α-Synuclein neurodegeneration can be blocked by modulation of neuroinflammatory processes through genetic knockout of MHC-II and Fcλ or through administration of the immunophilin ligand FK506 (30–32). Dopaminergic neurons in the SNpc appear to be particularly sensitive to proinflammatory cytokines, suggesting that the model used here is, at least in part, dependent on proinflammatory responses to kill dopaminergic neurons (33, 34). LRRK2 KO rodents show reduced proinflammatory responses in the brain in response to lipopolysaccharide or HIV-trans-activating protein administration (16, 35). One mechanism whereby LRRK2 kinase inhibitors could block α-synuclein-induced dopaminergic neurotoxicity could be reduction of inflammatory responses known to cause neurodegeneration of dopaminergic cells. Our observation of reduced microgliosis and recruitment of CD68 cells to the midbrain in G2019S-LRRK2 rats treated with PF-06447475 are consistent with this mechanism of action.

Viral coexpression of neuroprotective proteins in neurons can also block α-synuclein toxicity in dopaminergic SNpc neurons. These proteins include HSP70, parkin, PLK2, and Nedd4 (36–38). These proteins are associated with a diversity of cellular processes, including protein chaperone activity, mitochondrial maintenance, and synaptic function. LRRK2 may impair degradation of α-synuclein (39) or synergistically impair mitochondrial function together with α-synuclein (40). Because the species of α-synuclein that underlies dopaminergic neurodegeneration is not clear, it was not possible for us to definitively assess a direct effect of G2019S-LRRK2 expression on toxic α-synuclein isoforms. Because LRRK2 is expressed in both neurons and activated myeloid cells in the rats utilized in this study, the interaction between G2019S-LRRK2 and α-synuclein-induced dopaminergic neurodegeneration awaits further clarification in models that conditionally restrict LRRK2 expression and/or inhibition.

In our study, it is not clear whether the neurodegeneration associated with α-synuclein is prevented or delayed. Either way, a delay or a block of neurodegeneration associated with PD might represent a significant therapeutic advance. It will be important to define the therapeutic efficacy window of LRRK2 kinase inhibition with respect to the timing of LRRK2 kinase inhibition in the context of ongoing neurodegeneration and the level of LRRK2 kinase inhibition required for neuroprotective effects. These studies can be accomplished by varying the dosage of the LRRK2 kinase inhibitor to achieve different pharmacodynamic profiles and by initiating treatment at time points where neurodegenerative pathways have already commenced. Such data might be critical for the appropriate design of clinical trials for LRRK2 inhibitors in PD.

Small molecule kinase inhibitors have had tremendous therapeutic impact in a variety of disease in the last 25 years (41). Some of the challenges for LRRK2 kinase inhibitors include the definition of efficacy and further refinement of the mechanism of action in the models described here as well as other rodent models of PD, such as the recently described preformed fibril model of α-synuclein neurotoxicity (42). The tolerability and safety of LRRK2 kinase inhibitors needs further evaluation, particularly in non-human primates, and the means and outcomes to assess on-target LRRK2 inhibition and desired clinical effect in humans need to be identified.

Author Contributions—A. B. W. and W. D. H. conceived and coordinated the study and wrote the paper. J. P. L. D., H. A. A., X. H., L. A. V., M. S. M., K. B. F., E. N., and Y. C. designed, performed, and analyzed the experiments and edited the manuscript. S. J. S., P. G., and W. D. H. provided pharmacokinetic data and designed the experiments related to *in vivo* dosing. All authors analyzed the results and approved the final version of the manuscript.

Acknowledgments—We thank Jaclyn Henderson, Bethany Kormos, Karen Coffman, Chris Houle, and the other members of the Pfizer LRRK2 team. We also thank Rose Creed, Lindsay Stoyka, and Jonathan Blackburn for technical assistance.

References

1. Pringsheim, T., Jette, N., Frolkis, A., and Steeves, T. D. (2014) The prevalence of Parkinson's disease: a systematic review and meta-analysis. *Movement Disorders* **13,** 1583–1590
2. Braak, H., Del Tredici, K., Rüb, U., de Vos, R. A., Jansen Steur, E. N., and Braak, E. (2003) Staging of brain pathology related to sporadic Parkinson's disease. *Neurobiol. Aging* **24,** 197–211
3. Nalls, M. A., Pankratz, N., Lill, C. M., Do, C. B., Hernandez, D. G., Saad, M., DeStefano, A. L., Kara, E., Bras, J., Sharma, M., Schulte, C., Keller, M. F., Arepalli, S., Letson, C., Edsall, C., Stefansson, H., Liu, X., Pliner, H., Lee, J. H., Cheng, R., International Parkinson's Disease Genomics, C., Parkinson's Study Group Parkinson's Research: The Organized, G. I., andMe, GenePd, NeuroGenetics Research, C., Hussman Institute of Human, G., The Ashkenazi Jewish Dataset, I., Cohorts for, H., Aging Research in Ge-

netic, E., North American Brain Expression, C., United Kingdom Brain Expression, C., Greek Parkinson's Disease, C., Alzheimer Genetic Analysis, G., Ikram, M. A., Ioannidis, J. P., Hadjigeorgiou, G. M., Bis, J. C., Martinez, M., Perlmutter, J. S., Goate, A., Marder, K., Fiske, B., Sutherland, M., Xiromerisiou, G., Myers, R. H., Clark, L. N., Stefansson, K., Hardy, J. A., Heutink, P., Chen, H., Wood, N. W., Houlden, H., Payami, H., Brice, A., Scott, W. K., Gasser, T., Bertram, L., Eriksson, N., Foroud, T., and Singleton, A. B. (2014) Large-scale meta-analysis of genome-wide association data identifies six new risk loci for Parkinson's disease. *Nat. Genet.* **9,** 989–993

4. Singleton, A. B., Farrer, M., Johnson, J., Singleton, A., Hague, S., Kachergus, J., Hulihan, M., Peuralinna, T., Dutra, A., Nussbaum, R., Lincoln, S., Crawley, A., Hanson, M., Maraganore, D., Adler, C., Cookson, M. R., Muenter, M., Baptista, M., Miller, D., Blancato, J., Hardy, J., and Gwinn-Hardy, K. (2003) α-Synuclein locus triplication causes Parkinson's disease. *Science* **302,** 841
5. Healy, D. G., Falchi, M., O'Sullivan, S. S., Bonifati, V., Durr, A., Bressman, S., Brice, A., Aasly, J., Zabetian, C. P., Goldwurm, S., Ferreira, J. J., Tolosa, E., Kay, D. M., Klein, C., Williams, D. R., Marras, C., Lang, A. E., Wszolek, Z. K., Berciano, J., Schapira, A. H., Lynch, T., Bhatia, K. P., Gasser, T., Lees, A. J., Wood, N. W., and International LRRK2 Consortium (2008) Phenotype, genotype, and worldwide genetic penetrance of LRRK2-associated Parkinson's disease: a case-control study. *Lancet Neurol.* **7,** 583–590
6. West, A. B., Moore, D. J., Biskup, S., Bugayenko, A., Smith, W. W., Ross, C. A., Dawson, V. L., and Dawson, T. M. (2005) Parkinson's disease-associated mutations in leucine-rich repeat kinase 2 augment kinase activity. *Proc. Natl. Acad. Sci. U.S.A.* **102,** 16842–16847
7. Cookson, M. R. (2010) The role of leucine-rich repeat kinase 2 (LRRK2) in Parkinson's disease. *Nature Rev. Neurosci.* **11,** 791–797
8. Lin, X., Parisiadou, L., Gu, X. L., Wang, L., Shim, H., Sun, L., Xie, C., Long, C. X., Yang, W. J., Ding, J., Chen, Z. Z., Gallant, P. E., Tao-Cheng, J. H., Rudow, G., Troncoso, J. C., Liu, Z., Li, Z., and Cai, H. (2009) Leucine-rich repeat kinase 2 regulates the progression of neuropathology induced by Parkinson's-disease-related mutant α-synuclein. *Neuron* **64,** 807–827
9. Daher, J. P., Pletnikova, O., Biskup, S., Musso, A., Gellhaar, S., Galter, D., Troncoso, J. C., Lee, M. K., Dawson, T. M., Dawson, V. L., and Moore, D. J. (2012) Neurodegenerative phenotypes in an A53T α-synuclein transgenic mouse model are independent of LRRK2. *Hum. Mol. Genet.* **21,** 2420–2431
10. Herzig, M. C., Bidinosti, M., Schweizer, T., Hafner, T., Stemmelen, C., Weiss, A., Danner, S., Vidotto, N., Stauffer, D., Barske, C., Mayer, F., Schmid, P., Rovelli, G., van der Putten, P. H., and Shimshek, D. R. (2012) High LRRK2 levels fail to induce or exacerbate neuronal α-synucleinopathy in mouse brain. *PloS ONE* **7,** e36581
11. West, A. B., Cowell, R. M., Daher, J. P., Moehle, M. S., Hinkle, K. M., Melrose, H. L., Standaert, D. G., and Volpicelli-Daley, L. A. (2014) Differential LRRK2 expression in the cortex, striatum, and substantia nigra in transgenic and nontransgenic rodents. *J. Comp. Neurol.* **522,** 2465–2480
12. Walker, M. D., Volta, M., Cataldi, S., Dinelle, K., Beccano-Kelly, D., Munsie, L., Kornelsen, R., Mah, C., Chou, P., Co, K., Khinda, J., Mroczek, M., Bergeron, S., Yu, K., Cao, L. P., Funk, N., Ott, T., Galter, D., Riess, O., Biskup, S., Milnerwood, A. J., Stoessl, A. J., Farrer, M. J., and Sossi, V. (2014) Behavioral deficits and striatal DA signaling in LRRK2 p.G2019S transgenic rats: a multimodal investigation including PET neuroimaging. *J. Parkinsons Dis.* **4,** 483–498
13. Lee, J. W., Tapias, V., Di Maio, R., Greenamyre, J. T., and Cannon, J. R. (2015) Behavioral, neurochemical, and pathologic alterations in bacterial artificial chromosome transgenic G2019S leucine-rich repeated kinase 2 rats. *Neurobiol. Aging* **36,** 505–518
14. Kirik, D., Annett, L. E., Burger, C., Muzyczka, N., Mandel, R. J., and Björklund, A. (2003) Nigrostriatal α-synucleinopathy induced by viral vector-mediated overexpression of human α-synuclein: a new primate model of Parkinson's disease. *Proc. Natl. Acad. Sci. U.S.A.* **100,** 2884–2889
15. Oliveras-Salvá, M., Van der Perren, A., Casadei, N., Stroobants, S., Nuber, S., D'Hooge, R., Van den Haute, C., and Baekelandt, V. (2013) rAAV2/7 vector-mediated overexpression of α-synuclein in mouse substantia nigra induces protein aggregation and progressive dose-dependent neurodegeneration. *Mol. Neurodegener.* **8,** 44
16. Daher, J. P., Volpicelli-Daley, L. A., Blackburn, J. P., Moehle, M. S., and West, A. B. (2014) Abrogation of α-synuclein-mediated dopaminergic neurodegeneration in LRRK2-deficient rats. *Proc. Natl. Acad. Sci. U.S.A.* **111,** 9289–9294
17. Fuji, R. N., Flagella, M., Baca, M., MA, S. B., Brodbeck, J., Chan, B. K., Fiske, B. K., Honigberg, L., Jubb, A. M., Katavolos, P., Lee, D. W., Lewin-Koh, S. C., Lin, T., Liu, X., Liu, S., Lyssikatos, J. P., O'Mahony, J., Reichelt, M., Roose-Girma, M., Sheng, Z., Sherer, T., Smith, A., Solon, M., Sweeney, Z. K., Tarrant, J., Urkowitz, A., Warming, S., Yaylaoglu, M., Zhang, S., Zhu, H., Estrada, A. A., and Watts, R. J. (2015) Effect of selective LRRK2 kinase inhibition on nonhuman primate lung. *Sci. Transl. Med.* **7,** 273ra215
18. Baptista, M. A., Dave, K. D., Frasier, M. A., Sherer, T. B., Greeley, M., Beck, M. J., Varsho, J. S., Parker, G. A., Moore, C., Churchill, M. J., Meshul, C. K., and Fiske, B. K. (2013) Loss of leucine-rich repeat kinase 2 (LRRK2) in rats leads to progressive abnormal phenotypes in peripheral organs. *PloS ONE* **8,** e80705
19. Ness, D., Ren, Z., Gardai, S., Sharpnack, D., Johnson, V. J., Brennan, R. J., Brigham, E. F., and Olaharski, A. J. (2013) Leucine-rich repeat kinase 2 (LRRK2)-deficient rats exhibit renal tubule injury and perturbations in metabolic and immunological homeostasis. *PloS ONE* **8,** e66164
20. Kirik, D., Rosenblad, C., Burger, C., Lundberg, C., Johansen, T. E., Muzyczka, N., Mandel, R. J., and Björklund, A. (2002) Parkinson-like neurodegeneration induced by targeted overexpression of alpha-synuclein in the nigrostriatal system. *J. Neurosci.* **22,** 2780–2791
21. George, J. M., Jin, H., Woods, W. S., and Clayton, D. F. (1995) Characterization of a novel protein regulated during the critical period for song learning in the zebra finch. *Neuron* **15,** 361–372
22. Maroteaux, L., Campanelli, J. T., and Scheller, R. H. (1988) Synuclein: a neuron-specific protein localized to the nucleus and presynaptic nerve terminal. *J. Neurosci.* **8,** 2804–2815
23. Van der Perren, A., Toelen, J., Casteels, C., Macchi, F., Van Rompuy, A. S., Sarre, S., Casadei, N., Nuber, S., Himmelreich, U., Osorio Garcia, M. I., Michotte, Y., D'Hooge, R., Bormans, G., Van Laere, K., Gijsbers, R., Van den Haute, C., Debyser, Z., and Baekelandt, V. (2014) Longitudinal follow-up and characterization of a robust rat model for Parkinson's disease based on overexpression of alpha-synuclein with adeno-associated viral vectors. *Neurobiol. Aging* **3,** 1543–1558
24. Henderson, J. L., Kormos, B. L., Hayward, M. M., Coffman, K. J., Jasti, J., Kurumbail, R. G., Wager, T. T., Verhoest, P. R., Noell, G. S., Chen, Y., Needle, E., Berger, Z., Steyn, S. J., Houle, C., Hirst, W. D., and Galatsis, P. (2014) Discovery and preclinical profiling of 3-[4-(morpholin-4-yl)-7H-pyrrolo[2,3-d]pyrimidin-5-yl]benzonitrile (PF-06447475), a highly potent, selective, brain penetrant, and in vivo active LRRK2 kinase inhibitor. *J. Med. Chem.* **1,** 419–432
25. Kaufman, A. C., Salazar, S. V., Haas, L. T., Yang, J., Kostylev, M. A., Jeng, A. T., Robinson, S. A., Gunther, E. C., van Dyck, C. H., Nygaard, H. B., and Strittmatter, S. M. (2015) Fyn inhibition rescues established memory and synapse loss in Alzheimer mice. *Ann. Neurol.* **6,** 953–971
26. Moehle, M. S., Daher, J. P., Hull, T. D., Boddu, R., Abdelmotilib, H. A., Mobley, J., Kannarkat, G. T., Tansey, M. G., and West, A. B. (2015) The G2019S LRRK2 mutation increases myeloid cell chemotactic responses and enhances LRRK2 binding to actin-regulatory proteins. *Hum. Mol. Genet.* 10.1093/hmg/ddv157
27. West, A. B. (2014) Ten Years and counting: moving leucine-rich repeat kinase 2 inhibitors to the clinic. *Mov. Disord.* **2,** 180–189
28. Smith, W. W., Pei, Z., Jiang, H., Dawson, V. L., Dawson, T. M., and Ross, C. A. (2006) Kinase activity of mutant LRRK2 mediates neuronal toxicity. *Nat. Neurosci.* **9,** 1231–1233
29. Greggio, E., Jain, S., Kingsbury, A., Bandopadhyay, R., Lewis, P., Kaganovich, A., van der Brug, M. P., Beilina, A., Blackinton, J., Thomas, K. J., Ahmad, R., Miller, D. W., Kesavapany, S., Singleton, A., Lees, A., Harvey, R. J., Harvey, K., and Cookson, M. R. (2006) Kinase activity is required for the toxic effects of mutant LRRK2/dardarin. *Neurobiol. Dis.* **23,** 329–341
30. Van der Perren, A., Macchi, F., Toelen, J., Carlon, M. S., Maris, M., de Loor, H., Kuypers, D. R., Gijsbers, R., Van den Haute, C., Debyser, Z., and Baekelandt, V. (2015) FK506 reduces neuroinflammation and dopaminergic neurodegeneration in an alpha-synuclein-based rat model for Parkinson's disease. *Neurobiol. Aging* **3,** 1559–1568

31. Harms, A. S., Cao, S., Rowse, A. L., Thome, A. D., Li, X., Mangieri, L. R., Cron, R. Q., Shacka, J. J., Raman, C., and Standaert, D. G. (2013) MHCII is required for α-synuclein-induced activation of microglia, CD4 T cell proliferation, and dopaminergic neurodegeneration. *J. Neurosci.* **33,** 9592–9600
32. Cao, S., Standaert, D. G., and Harms, A. S. (2012) The γ chain subunit of Fc receptors is required for α-synuclein-induced pro-inflammatory signaling in microglia. *J. Neuroinflamm.* **9,** 259
33. Chakrabarty, P., Ceballos-Diaz, C., Lin, W. L., Beccard, A., Jansen-West, K., McFarland, N. R., Janus, C., Dickson, D., Das, P., and Golde, T. E. (2011) Interferon-γ induces progressive nigrostriatal degeneration and basal ganglia calcification. *Nat. Neurosci.* **14,** 694–696
34. Harms, A. S., Barnum, C. J., Ruhn, K. A., Varghese, S., Treviño, I., Blesch, A., and Tansey, M. G. (2011) Delayed dominant-negative TNF gene therapy halts progressive loss of nigral dopaminergic neurons in a rat model of Parkinson's disease. *Mol. Ther.* **19,** 46–52
35. Puccini, J. M., Marker, D. F., Fitzgerald, T., Barbieri, J., Kim, C. S., Miller-Rhodes, P., Lu, S. M., Dewhurst, S., and Gelbard, H. A. (2015) Leucine-rich repeat kinase 2 modulates neuroinflammation and neurotoxicity in models of human immunodeficiency virus 1-associated neurocognitive disorders. *J. Neurosci.* **35,** 5271–5283
36. Moloney, T. C., Hyland, R., O'Toole, D., Paucard, A., Kirik, D., O'Doherty, A., Gorman, A. M., and Dowd, E. (2014) Heat shock protein 70 reduces α-synuclein-induced predegenerative neuronal dystrophy in the α-synuclein viral gene transfer rat model of Parkinson's disease. *CNS Neurosci. Ther.* **20,** 50–58
37. Oueslati, A., Schneider, B. L., Aebischer, P., and Lashuel, H. A. (2013) Polo-like kinase 2 regulates selective autophagic α-synuclein clearance and suppresses its toxicity *in vivo*. *Proc. Natl. Acad. Sci. U.S.A.* **110,** E3945–E3954
38. Lo Bianco, C., Ridet, J. L., Schneider, B. L., Deglon, N., and Aebischer, P. (2002) α-Synucleinopathy and selective dopaminergic neuron loss in a rat lentiviral-based model of Parkinson's disease. *Proc. Natl. Acad. Sci. U.S.A.* **99,** 10813–10818
39. Orenstein, S. J., Kuo, S. H., Tasset, I., Arias, E., Koga, H., Fernandez-Carasa, I., Cortes, E., Honig, L. S., Dauer, W., Consiglio, A., Raya, A., Sulzer, D., and Cuervo, A. M. (2013) Interplay of LRRK2 with chaperone-mediated autophagy. *Nat. Neurosci.* **16,** 394–406
40. Cherra, S. J., 3rd, Steer, E., Gusdon, A. M., Kiselyov, K., and Chu, C. T. (2013) Mutant LRRK2 elicits calcium imbalance and depletion of dendritic mitochondria in neurons. *Am. J. Pathol.* **182,** 474–484
41. Fabbro, D. (2014) 25 years of small molecular weight kinase inhibitors: potentials and limitations. *Mol. Pharmacol.* **5,** 766–775
42. Luk, K. C., Kehm, V., Carroll, J., Zhang, B., O'Brien, P., Trojanowski, J. Q., and Lee, V. M. (2012) Pathological α-synuclein transmission initiates Parkinson-like neurodegeneration in nontransgenic mice. *Science* **338,** 949–953